RSC Advances

ROYAL SOCIETY OF CHEMISTRY

www.rsc.org/advances

Journal Name

ARTICLE

Ten-fold coordinated polymorph and metallization of TiO_2 under high pressure

Received 00th January 20xx,
Accepted 00th January 20xx

DOI: 10.1039/x0xx00000x

www.rsc.org/

Xin Zhong[a], Jianyun Wang[a], Shoutao Zhang[a], Guochun Yang[a,b,]* and Yanchao Wang[a,]*

Titanium dioxide (TiO_2) has a wide range of industrial applications (e.g., photocatalysis and solar cells). Pressure causes profound structural and electronic changes of TiO_2, leading to the fundamental modification of its physical properties. We here report the metallization of TiO_2 at high pressure through first-principles swarm structure searching calculations. Metallization accompanies the stabilization of a body-centered tetragonal CaC_2-type structure (space group *I4/mmm*), which is more stable than the Fe_2P-type structure above 690 GPa. This phase adopts a ten-fold coordinated structure consisted of face-sharing TiO_{10} dodecahedrons, the highest coordination number among all TiO_2 phases known so far. In contrast to the nine-fold Fe_2P-type structure, the higher coordination and denser polyhedral packing makes the CaC_2-type structure energetically favorable. Our work enables an opportunity for understanding the structure and electronic property of TiO_2 at high pressure.

1 Introduction

Titanium dioxide (TiO_2) is of particular interest due to its versatile physical and chemical properties. Therefore, it has extensively been used in a wide variety of applications including pigment,[1] photocatalysis,[2] solar cells,[3] electrochemistry,[4] dynamic random access memory modules,[5] and ceramic industries.[6] In particular, the structure and property of TiO_2 are strongly dependent on the specific environment. Various polymorphs have been observed under varying chemical, temperature, and pressure conditions. High-pressure phase transitions of TiO_2 have attracted special attention because these phases exhibit unusual properties (e.g. ultrahard and ultrastiff,[7-8] a quasi-direct band gap character,[9] unusual compression behavior[10]). In addition, high-pressure phase transitions of TiO_2 can be regarded as a lower-pressure analogy of SiO_2, the most abundant component of the Earth's mantle.[8] Pressure-induced phase transitions of TiO_2 also serve as analogues of the structures adopted in many other important AX_2 compounds.[8, 11] Recently, structural behaviour and mechanical property of nanocrystalline TiO_2 under pressure has been extensively investigated.[12-14] It is found that the bulk modulus of a nano TiO2 sample strongly depends on the particle size.

TiO_2 has a rich phase diagram under high pressure.[8, 11, 15-16] Up to now, at least 8 solid phases have been identified. Specifically, the rutile and anatase phases transform to a columbite (α-PbO_2) form between 4.5 and 7 GPa,[17] and then to a baddeleyite structure (ZrO_2) at around 20 GPa,[18-19] then to an brookite phase (space group *Pbca*)[8], followed by a cotunnite structure with *Pnma* symmetry.[8, 19-21] Recently, first-principles calculations predicted a new phase of TiO_2 with $Pca2_1$ symmetry at around 50 GPa,[10, 22] although it has not been found experimentally. Up to now, the highest pressure phase of TiO_2 identified is the Fe_2P-type (*P*-62*m*) structure at 210 GPa,[11] which was found to have the smallest band gap and the highest coordination number (nine-fold) among the known TiO_2 phases. It is well known that high pressure can tune the band gap and induce insulator or semiconductor to metal phase transition.[11, 23-25] Light absorption of TiO_2 can be enhanced by reducing its band gap or metallization. This is a necessary premise for improving the photocatalytic activity of TiO_2.[26-28] In particular, pressured induced metallization of TiO_2 has not been reported thus far.

For this purpose, we have extensively explored the high-pressure phases of TiO_2 by using unbiased structure searching techniques and first-principles density functional calculations. We discovered a novel tetragonal CaC_2-type structure with *I*4/*mmm* symmetry stable above 690 GPa consisting of a ten-fold coordination of Ti atom. It is found that there are significant differences in the electronic properties between Fe_2P-type and CaC_2-type structures.

2 Computational details

Our structure searching simulations are performed through the in-house developed CALYPSO structure prediction method based on a particle swarm optimization algorithm via a global minimization of free energy surfaces merging *ab initio* total energy calculations as implemented in the CALYPSO code.[29-30] The most remarkable feature of this methodology is the capability of predicting the

---

[a] *State Key Laboratory of Superhard Materials, Jilin University, Changchun 130012, China. E-mail: wyc@calypso.cn*
[b] *Faculty of Chemistry, Northeast Normal University, Changchun 130024, China. E-mail: yanggc468@nenu.edu.cn*

† Footnotes relating to the title and/or authors should appear here.

Electronic Supplementary Information (ESI) available: [The validity of pseudopotentials, phonon dispersion curves, electron localization function, and the calculated energy and volume per formula unit as a function of pressure, and the main structural parameters]. See DOI: 10.1039/x0xx00000x ground-state structure with only the knowledge of chemical composition. Our method has been benchmarked on various known systems, ranging from elements to binary and ternary compounds.[29, 31-34] The underlying *ab initio* structural relaxations and electronic band structure calculations were performed in the framework of density functional theory within the Perdew–Burke–Ernzerhof parameterization[35] as implemented in the VASP (Vienna *Ab Initio* simulation package) code.[36] The electron-ion interaction was described by projected-augmented-wave potentials with $3d^2 4s^2 3p^6 3s^2$ and $2s^2 2p^4$ as valence electrons for Ti and O, respectively. The use of the plane-wave kinetic energy cutoff of 1000 eV and Monkhorst−Pack k-meshes with grid spacing of $2\pi \times 0.03$ Å^{-1} were chosen to ensure that all the enthalpy calculations are well converged to better than 1 meV/atom. The validity of the used PAW potential at currently studied pressures (< 700 GPA) has earlier been carefully checked (Fig. S1) by comparing with full-potential linearized augmented plane wave (FP-LAPW) method as implemented in the ELK code.[37] The phonon calculations were performed to determine the dynamical stability through supercell method as implemented in the PHONOPY code.[38] It is noted that all calculations have been made at 0 K.

3 Results and discussion

Structure predictions through the CALYPSO code with 1-4 formula units (f.u.) per simulation cell were performed at pressure range of 0–800 GPa. The experimental structures were all successfully reproduced, validating our methodology in application to dense TiO_2. The calculated enthalpies per formula unit as a function of pressure with respect to Fe_2P-type structure are plotted in Fig. 1. At low pressure regions, our simulations readily found rutile and anatase phases at ambient pressure. With increasing the pressure, our simulations found the columbite (α-PbO_2), baddeleyite (ZrO_2), OI (Pbca) and Cotunnite (Pnma) structures proposed earlier. For the Post-Cotunnite regions, the *Pnma* structure transforms to Fe_2P-type (*P*-62*m*) structure. The calculated transition pressures for these phases along with other calculated and experimental data were given in Table 1. It is found that our results are in reasonable agreement with the previous calculations.[11] The slight difference between calculation and measurement might originate from the temperature effect, which is not considered in our calculation. Moreover, the experimental structural parameters are also well reproduced by our calculations (Table S1), supporting on the validity of pseudopotentials adopted in this work.

With increasing pressure, we indentify a body-centered tetragonal CaC_2[39] or BaO_2-type[40] structure (space group *I4/mmm*, two formula units per cell, see Fig. 2b) that become energetically favorable at ~690 GPa. Interestingly, the CaC_2-type structure consists of face-sharing Ti-O dodecahedrons. Each Ti atom is centered in dodecahedron to form ten-fold binding with O having eight of the Ti-O distances being 1.80 Å and the other two 1.79 Å. This is the highest coordination number among the known TiO_2 phases. It should be noted that the distance between the two nearest oxygen atoms is 1.76 Å. It means that this structure does not contain dumbbell carbon and oxygen as observed in CaC_2[36] and BaO_2-type[37]. The phonon dispersive curves confirm that the *I4/mmm* structure is dynamically stable (Fig. S2). The CaC_2-type phase is structurally very distinct from Fe_2P-type consisting of fairly regular TiO_9 tricapped trigonal prisms with a closely compact lattice (Fig. 2a). Ti-O distances in Fe_2P-type structure are slightly shorter (1.64 and 1.79 Å) than those in CaC_2-type.

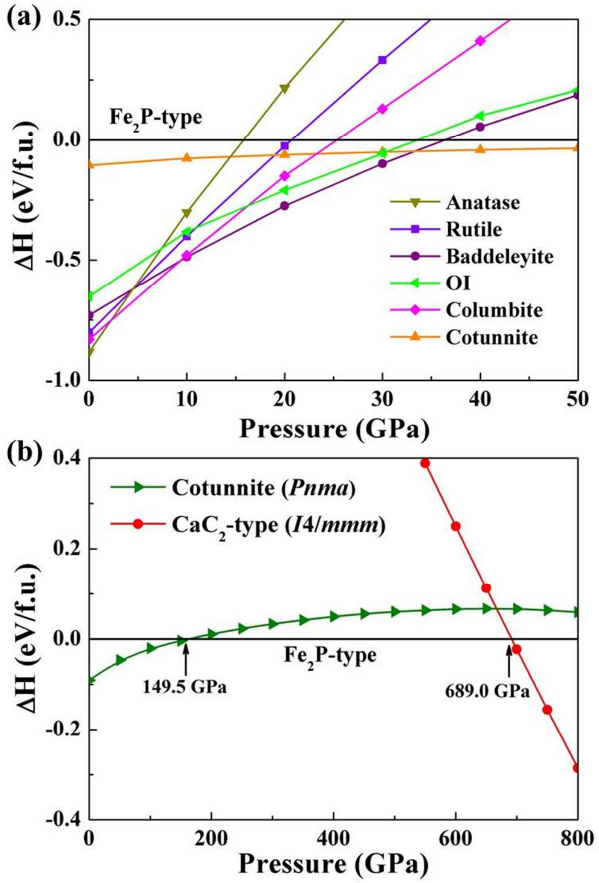

Fig. 1 The relative enthalpy per formula unit with respect to Fe_2P-type structure as a function of pressure within PBE calculations at T = 0 K. (a) is for the pressure regime between 0 and 50 GPa, and (b) for the high-pressure post-cotunnite regime.

Table 1. Computed transition pressures (GPa) for thee considered phases, as compared to experimental and other theoretical data.

Phase	Space group	Transition pressure
Anatase	*I*4$_1$/*amd*	This work 0.0 GPa Other calc. 0. 0GPa[41]
Columbite	*Pbcn*	This work 3.5 GPa Other calc. 3.0 GPa[41]
Baddeleyite	*P*2$_1$/*c*	This work 11.5 GPa Expt. 20.0 GPa[42] Other calc. 12.0 GPa[41]
Cotunnite	*Pnma*	This work > 33.5 GPa Expt. 48-56 GPa, 1800 K[43] Other calc. 40.0 GPa[41]
Fe_2P-Type	*P*-62*m*	This work 149.5 GPa Other calc. 147.0 GPa[44]
CaC_2-type	*I*4/*mmm*	This work 689.0 GPa

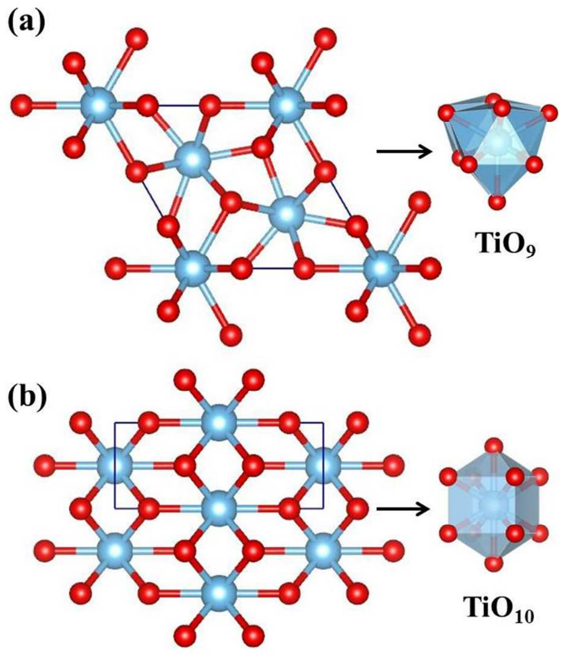

Fig. 2 Crystal structures for the Fe_2P-type (a) and CaC_2-type (b) of TiO_2 at 700 GPa. Small and large spheres represent O and Ti atoms, respectively. The lattice parameters for the Fe_2P-type structure are $a = b = 4.3833$ Å and $c = 2.3868$ Å. The atomic coordinates are Ti (1a) (0, 0, 0), Ti (2d) (0.333, 0.667, 0.5), O (3g) (0, 0.259, 0.5), and O (3f) (0.406, 0.406, 0). The lattice parameters for the CaC_2-type structure are $a = b = 2.1985$ Å and $c = 5.3617$ Å. The atomic coordinates are Ti (2b) (0, 0, 0.5) and O (4e) (0, 0, 0.837), respectively.

To analyze the Ti-O bonding character and phase mechanism, electron localization function (ELF)[45] and Bader charge[46] of the Fe_2P-type and CaC_2-type structures are calculated. Analysis of the ELF for CaC_2-type structures shows a very small value (~0.23) between Ti and O atoms (Fig. S3), which is typical for ionic and metallic bonding.[47] The calculated Bader charges are +1.74 and −0.87e on the Ti and O atoms, respectively. This results show that Ti-O is ionic bonding and corresponds to an ionicity of ~43%. In Fe_2P-type, the charges on the Ti and O atoms, obtained from the Bader charge analysis, are +1.99 and −0.99e, respectively. This equates to an ionicity of ~50%. Obviously, ionicity in CaC_2-type is smaller than that in Fe_2P-type. In general, structures with lower ionic are less sensitive to the Coulomb interactions between neighboring atoms. Thus, the stabilizing effect in CaC_2-type is less remarkable than this in Fe_2P-type. This is also consistent with the longer Ti-O distances in CaC_2-type. At certain pressure p, the structure with the lowest enthalpy $H = U + pV$ is the most stable, where U and V are the energy and volume per formula unit, respectively.[48] In general, structures with smaller volumes are favorable at high pressure. Variation of the unit cell volume as a function of pressure for the Fe_2P-type and CaC_2-type structures were shown in Fig. 3. It is found that the CaC_2-type unit cell volume is smaller than that of Fe_2P-type. This phase transition reduces the volume by ~3.37% relative to the Fe_2P-type structure, which amounts to a lowering of the pV term in the enthalpy of ~1.86 eV per formula unit (Fig. S4a). However, U of the CaC_2-type is larger than this of Fe_2P-type (Fig. S4b), which is also agreement with the above ionic analysis. In combination of U and pV terms, CaC_2-type is energetically favorable above 690 GPa (Fig. 1b). Those indicates that the lower (tetragonal) symmetry unit cell of the CaC_2-type structure become much denser and stable than the hexagonal one at the transition pressure, which is attributed to the higher coordination and denser polyhedral packing.

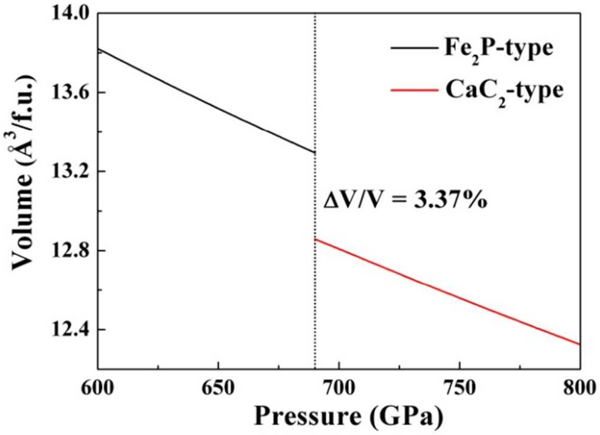

Fig. 3 Variation of the unit cell volume as a function of pressure for the Fe_2P-type and CaC_2-type structures. Vertical dotted line indicates the transition pressure.

Subsequently, we investigated the effect of pressure on the band gaps for Fe_2P-type and CaC_2-type structures, respectively (Fig. 4). The band gaps of the Fe_2P-type structure gradually decrease with increasing pressure. Among the known TiO_2 polymorphs, the Fe_2P-type structure was found to have the smallest band gap (0.66 eV at 160 GPa),[11] which compares well with our value of 0.62 eV. Above 160 GPa, the band gap is further reduced. However, pressure-induced metallization are not observed until the CaC_2-type transition at ~690 GPa. It is interesting to find that CaC_2-type structure is metallic over the whole studied pressure range. The electronic band structure and projected density of states (PDOS) at 700 GPa for the Fe_2P-type and CaC_2-type structures were shown in Fig. 5. For the CaC_2-type structure, the valence band is predominantly O 2p in character, with a small contribution from the Ti 3d components. While the conduction band is mainly composed of Ti 3d components mixed with a small contribution from the O 2p. The valence band composition for the Fe_2P-type is similar to those of in CaC_2-type. Notably, Ti 3d components mainly contribute to the conduction band. This character is mainly responsible for the band gap narrowing in Fe_2P-type.[11] It should be noted that this transition pressure (690 GPa) for the CaC_2-type structure is unrealistic for present experimental techniques, which might help to trigger new experimental development.

There appear large dispersion bands crossing the Fermi level (E_F) and a flat band in the vicinity of E_F close to the Γ point. The simultaneous occurrence of "flat band-steep band"[49-50] near the Fermi level is considered as favourable conditions for enhancing electron pairing, which is essential to superconducting behaviour. This character promotes our interests to investigate its superconductive behaviour. The calculated logarithmic phonon momentum $\omega_{\log}$ and electron–phonon coupling parameter λ are 1384.4 K and 0.23, respectively. Using the Allen and Dynes modified MaMillan formula,[51] the estimated superconducting transition temperature T_c is 0.03 K (taking value of 0.1 for the effective Coulomb repulsion parameter μ*), which is ascribed to the rather weak electron–phonon coupling.

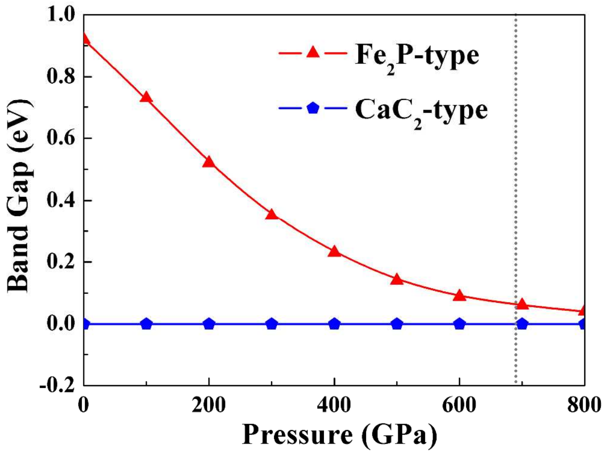

Fig. 4 Pressure dependence of band gaps of the Fe$_2$P-type and CaC$_2$-type structures. The vertical dotted line represents the phase transition pressure, which is also the metallization pressure.

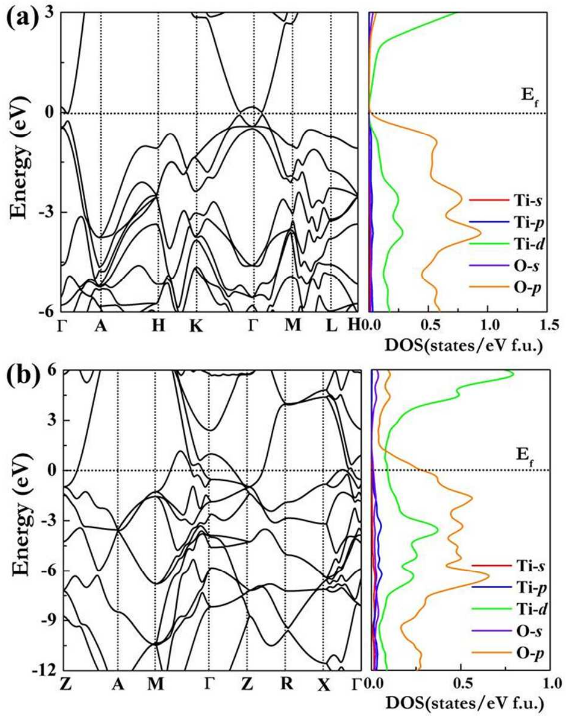

Fig. 5 Electronic band structure and projected density of states for the Fe$_2$P-type (a) and CaC$_2$-type (b) of TiO$_2$ at 700 GPa. The horizontal dashed line indicates the calculated Fermi energy.

4 Conclusions

In summary, a novel ten-coordinated TiO$_2$ polymorph with CaC$_2$-type symmetry has been predicted through first-principles swarm structure searching calculations. This phase become thermodynamically stable above ~690 GPa, and was found to be up to ~3.4% denser than that of the Fe$_2$P-type structure. It is found that ionicity in CaC$_2$-type is smaller than that in Fe$_2$P-type. Therefore, the favourable energetics of CaC$_2$-type mainly originates from close packing. Fe$_2$P-type and CaC$_2$-type structures have distinct electronic band structures and the metallization of TiO$_2$ occurs concomitantly with the phase transition to CaC$_2$-type. We hope that this work will stimulate further theoretical and experimental studies of TiO$_2$ at high pressure.

Acknowledgments

The authors acknowledge the funding supports from China 973 Program under Grant No. 2011CB808200, National Natural Science Foundation of China under Grant No. 11274136, 2012 Changjiang Scholar of Ministry of Education, and the Natural Science Foundation of Jilin Province (20150101042JC) and the Postdoctoral Science Foundation of China under grant 2013M541283.

Notes and references

[1] Y. Li, X. Zou, X. Huang, J. Shi, J. Zhao, H. Mel, H. Limin, *Biosens. Bioelectron.* **2015**, *67*, 35-41.

[2] R. Asahi, T. Morikawa, T. Ohwaki, K. Aoki, Y. Taga, *Science (New York, N.Y.)* **2001**, *293*, 269-271.

[3] Y. Bai, I. Mora-Sero, F. De Angelis, J. Bisquert, P. Wang, *Chem. Rev.* **2014**, *114*, 10095-10130.

[4] E. T. D. Kumar, V. Ganesh, *Chemelectrochem* **2014**, *1*, 590-600.

[5] W. Jeon, H. Chung, D. Joo, S. Kang, *Electrochem. Solid-State Lett.* **2008**, *11*, H19-H21.

[6] J. O. Carneiro, V. Teixeira, S. Azevedo, F. Fernandes, J. Neves, *J. Nanopart. Res.* **2012**, *18-19*, 165-176.

[7] L. S. Dubrovinsky, N. A. Dubrovinskaia, V. Swamy, J. Muscate, N. M. Harrison, R. Ahuja, B. Holm, B. Johansson, *Nature* **2001**, *410*, 653-654.

[8] N. A. Dubrovinskaia, L. S. Dubrovinsky, R. Ahuja, V. B. Prokopenko, V. Dmitriev, H. P. Weber, J. M. Osorio-Guillen, B. Johansson, *Phys. Rev. Lett.* **2001**, *87*, 275501.

[9] T. Zhu, S. Gao, *J. Phys. Chem. C* **2014**, *118*, 11385-11396.

[10] X. Zhou, X. Dong, G. Qian, L. Zhang, Y. Tian, H. Wang, *Phys. Rev. B* **2010**, *82*, 060102.

[11] H. Dekura, T. Tsuchiya, Y. Kuwayama, J. Tsuchiya, *Phys. Rev. Lett.* **2011**, *107*, 045701.

[12] H. Zhang, J. Banfield, *Chem. Rev.* **2014**, *114*, 9613-9644.

[13] Y. Al-Khatatbeh, K. Lee, B. Kiefer, *J. Phys. Chem. C* **2012**, *116*, 21635-21639.

[14] C. Popescu, J. Angel Sans, D. Errandonea, A. Segura, R. Villanueva, F. Sapina, *Inorganic Chemistry* **2014**, *53*, 11598-11603.

[15] J. Haines, J. M. Léger, *Physica (Amsterdam)* **1993**, *192B*, 232-239

[16] J. K. Dewhurst, J. E. Lowther, *Phys. Rev. B* **1996**, *54*, R3673-R3675.

[17] J. Staun Olsen, L. Gerward, J. Z. Jiang, *J. Phys. Chem. Solids* **1999**, *60*, 229-233
[18] H. Sato, S. Endo, M. Sugiysma, T. Kikegawa, O. Shimomura, *Science* **1991**, *251*, 786-788.
[19] J. Muscat, V. Swamy, N. M. Harrison, *Phys. Rev. B* **2002**, *65*, 224112.
[20] R. Ahuja, L. S. Dubrovinsky, *J. Phys.: Condens. Matter.* **2002**, *14*, 10995
[21] X. Wu, E. Holbig, G. Steinle-Neumann, *J. Phys.: Condens. Matter.* **2010**, *22*, 295501
[22] V. Swamy, N. C. Wilson, *J. Phys. Chem. C* **2014**, *118*, 8617-8625.
[23] I. Zardo, S. Yazji, C. Marini, E. Uccelli, M. Fontcuberta, A., G. Abstreiter, P. Postorino, *Acs. Nano.* **2012**, *6*, 3284-3291.
[24] L. Hromadova, R. Martonak, E. Tosatti, *Phys. Rev. B* **2013**, *87*, 144105.
[25] Z. Zhao, S. Wang, H. Zhang, W. Mao, *Phys. Rev. B* **2013**, *88*, 024120.
[26] J. Tao, T. Luttrell, M. Batzill, *Nat. Chem.* **2011**, *3*, 296-300.
[27] M. Khan, S. Ansari, D. Pradhan, M. Ansari, D. Han, J. Lee, M. Cho, *J. Mater. Chem. A* **2014**, *2*, 637-644.
[28] A. V. Rosario, E. C. Pereira, *Applied Catalysis B-Environmental* **2014**, *144*, 840-845.
[29] Y. Wang, J. Lv, L. Zhu, Y. Ma, *Phys. Rev. B* **2010**, *82*, 094116.
[30] Y. Wang, J. Lv, L. Zhu, Y. Ma, *Comput. Phys. Commun.* **2012**, *183*, 2063-2070.
[31] J. Lv, Y. Wang, L. Zhu, Y. Ma, *Phys. Rev. Lett.* **2011**, *106*, 015503.
[32] L. Zhu, H. Wang, Y. Wang, J. Lv, Y. Ma, Q. Cui, Y. Ma, G. Zou, *Phys. Rev. Lett.* **2011**, *106*, 145501.
[33] Y. Wang, H. Liu, J. Lv, L. Zhu, H. Wang, Y. Ma, *Nat. Commun.* **2011**, *2*.
[34] L. Zhu, H. Liu, C. J. Pickard, G. Zou, Y. Ma, *Nat. Chem.* **2014**, *6*, 644-648.
[35] J. P. Perdew, J. A. Chevary, S. H. Vosko, K. A. Jackson, M. R. Pederson, D. J. Singh, C. Fiolhais, *Phys. Rev. B,* **1992**, *46*, 6671-6687.
[36] G. Kresse, J. Furthmuller, *Phys. Rev. B,* **1996**, *54*, 11169-11186.
[37] J. Kunes, R. Arita, P. Wissgott, A. Toschi, H. Ikeda, K. Held, *Comp. Phys. Commun.* **2010**, *181*, 1888–1895.
[38] A. Togo, F. Oba, I. Tanaka, *Phys. Rev. B* **2008**, *78*, 134106.
[39] E. Ruiz , P. Alemany, *J. Phys. Chem.* **1995**, *99*, 3114-3119.
[40] W. Wong-Ng, R. S. Roth, *Physica C* **1994**, *233*, 97-101.
[41] X. G. Ma, P. Liang, L. Miao, S. W. Bie, C. K. Zhang, L. Xu, J. J. Jiang, *Phys. Status Solid B* **2009**, *246*, 2132.
[42] H. SATO, S. ENDO, M. SUGIYAMA, T. KIKEGAWA, O. SHIMOMURAK., KUSABA, *Science* **1991**, *251*, 786.
[43] Y. Al-Khatatbeh, K. K. M. Lee, B. Kiefer, *Phys. Rev. B* **2009**, *79*, 134114.
[44] Z. Fu, Y. Liang, S. Wang, Z. Zhong, *Phys. Status Solid B* **2013**, *250*, 2206.
[45] A. D. Becke, K. E. Edgecombe, *J. Chem. Phys.* **1990**, *92*, 5397-5403
[46] R. Bader, Atoms in Molecules: A Quantum Theory, Oxford University Press, New York, 1990.
[47] U. Haussermann, S. Wengert, P. Hofmann, A. Savin, O. Jepsen, R. Nesper, *Angew. Chem. Int. Ed.* **1994**, *33*, 2069-2073.
[48] C. J. Pickard, R. J. Needs, *Nature Materials* **2008**, *7*, 775-779.
[49] J. S. Tse, Y. Yao, K. Tanaka, *Phys. Rev. Lett.* **2007**, *98*, 117004.
[50] Y. W. Li, J. Hao, H. Liu, Y. Li, Y. M. Ma, *J. Chem. Phys.* **2014**, *140*, 174712.
[51] P. B. Allen, R. C. Dynes, *Phys. Rev. B* **1975**, *12*, 905-922.

Table of Contents Graphic

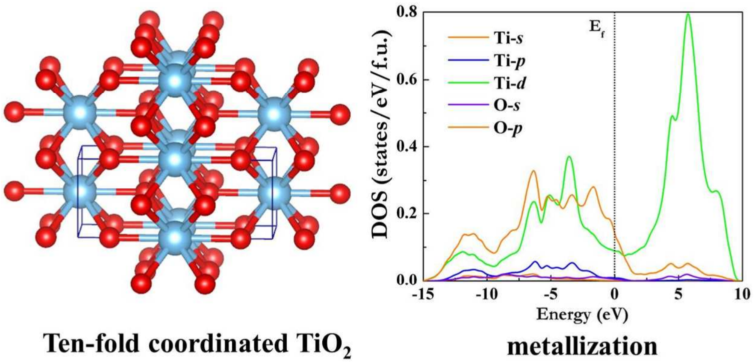

Ten-fold coordinated TiO_2 metallization

Text for TOC: A stable and metallic CaC_2-type structure of TiO_2 is identified with the highest coordination number among the known phases.